ACS OMEGA

http://pubs.acs.org/journal/acsodf

Article

Preparation and Comprehensive Performance Test of Superhydrophobic Paper Mulch Films

Anling Li, Yaohui Zhao, Shuaiyang Ren, Fangyuan Zhang, Fengwei Zhang,* and Qiang He*

Cite This: *ACS Omega* 2021, 6, 24407−24418

Read Online

ACCESS | Metrics & More | Article Recommendations

ABSTRACT: Paper mulch was treated with nano-zinc oxide and nano-silica dispersion by a brushing method, and its mechanical stability, hydrophobicity, impermeability, and wet strength were verified. The experiment shows that the mulch film after brushing has superhydrophobic properties, and it can also have better superhydrophobic properties and stability after being allowed to stand at room temperature for 240 h and drying under a vacuum of 0.03 MPa under negative pressure. The wet strength test after soaking for different times shows that the mechanical properties of the base paper are reduced more than that of the hydrophobic paper. It is concluded that the hydrophobic coating can improve the wet strength of the paper mulch. The experimental results show that the coating has the erosion durability and mechanical stability of the paper mulch, the wet strength can improve, and the paper mulch has stronger mechanical stability and stronger ability to adapt to complex environments.

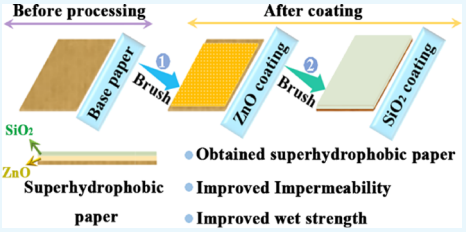

1. INTRODUCTION

In today's agricultural development, plastic mulch plays an increasingly important role. Mulch films not only play an important role in improving crop yield and water use efficiency but also play an active role in improving crop quality. Common traditional mulch films are mainly nondegradable polyethylene plastic mulch. Polyethylene plastic mulch films have good antipermeability and durability, but due to the low overall recovery rate, residual plastic films will accumulate in the soil with the passage of time, which will destroy the farmland soil structure, further reduce the soil permeability, and hinder the growth of crop roots; on the contrary, it will adversely lead to crop yield reduction. Because of the problem that the mulch film is difficult to degrade, agricultural production has been plagued, and the self-biodegradable mulch film has conveniently entered people's field of vision.

Due to the urgent need of agricultural production, scholars at home and abroad are increasingly inclined to study degradable and environment-friendly bio-mulch films. For example, Rocha et al.[1] reported a preparation method of a degradable bio-mulch film, in which a PBAT/polylactic acid composite was prepared by melt extrusion, and $CaCO_3$ with different contents was added to prepare a flexible film with lower cost and higher tensile strength. Zhang et al.[2] reported a preparation method of a degradable paper mulch film. A biodegradable mulch film paper was prepared by using pea starch and kraft paper as raw materials. The mulch film paper is 100% biodegradable and environment-friendly, has good mechanical properties, and better adapts to the production environment. La Fuente et al.[3] reported the preparation of a biodegradable mulch film. The biodegradable film was prepared from ozone-modified cassava starch with different concentrations. Films made of ozonated cassava starch have more uniform morphology, higher tensile strength, Young's modulus, and lower elongation. Although these films can be degraded, they all have the problems of difficult processing and poor mechanical properties and water resistance. Compared with paper-based films, they have the advantages of low cost, cheapness, and easily available raw materials and are more suitable for practical agricultural production. Compared with the problem that plastic mulch is difficult to degrade in soil and will pollute the environment, paper mulch will automatically degrade into inorganic substances such as water and carbon dioxide in the process of field mulch, which makes paper mulch have a better application prospect in soil environmental protection compared with plastic mulch. However, compared with the plastic mulch film, the paper-based mulch film also has some shortcomings. In the actual production, a paper mulching film surface is prone to pits, and rain water is easy to accumulate. It is inevitable that there will be rain soaking and tearing, and the paper mulch film has shortcomings in impermeability, durability, wet strength, and mechanical stability, which affect its service life. To improve this problem and make the paper-based film better used in practical

Received: May 19, 2021
Accepted: August 6, 2021
Published: September 14, 2021

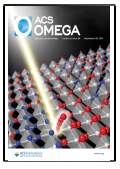

agricultural production, some scholars began to apply superhydrophobic materials to the paper-based film to improve its performance.

Generally, the wettability of liquid on a solid surface is mainly evaluated by two parameters, contact angle and angle hysteresis.[4] A superhydrophobic phenomenon refers to a special phenomenon in which water droplets exhibit a higher apparent contact angle (generally greater than 150°) and a lower angle hysteresis (generally less than 10°) on the solid surface.[5−9] A superhydrophobic phenomenon is mainly related to the microscopic rough structure of the material surface and its low surface energy.[10] Therefore, there are two main ways to prepare a superhydrophobic surface: one is to construct a certain rough structure on the surface of a low surface energy material, and the other is to cover the surface of a suitable material with a low surface energy material. At present, many preparation methods of a microstructure surface have appeared in the field of superhydrophobic preparation, such as deposition method,[11] phase separation method,[12] template method,[13] sol−gel method,[14] electrochemical deposition,[15] chemical etching method,[16] anodic oxidation method,[17] etc. Combined superhydrophobic materials and paper base more and more get the favor of scholars, such as Li et al.[18] who used a plasma etching method to prepare a paper surface with extremely high wettability, which can prevent various liquids from wetting the paper surface. Wen et al.[19] adopted a simple and environment-friendly superhydrophobic preparation method. Color super hydrophobic paper was obtained by precipitating cellulose and color stearate on swollen cotton, and the hydrophobic paper still maintained good hydrophobic stability after abrasion. Zhang et al.[20] reported a preparation method of superhydrophobic paper. By coating the mixture of silica nanoparticles and polystyrene-polymethyl methacrylate copolymer (PS-*co*-PMMA), flexible lightweight superhydrophobic paper with strong hydrophobicity was successfully prepared with excellent hydrophobic performance. Wang et al.[21] reported a method of preparation of superhydrophobic paper by in situ hydrolysis of tetraethyl titanate natural wood cellulose fiber made of superhydrophobic paper; the process without any chemical pretreatment, by adjusting the amount of acetic acid, can control the surface micro/nanoform and obtain the static water CA of 152.3° for superhydrophobic paper. In addition, this hydrophobic paper also has good self-cleaning performance and mechanical durability.

In addition, although there are many methods for preparing a superhydrophobic surface, most of them generally have problems such as high cost and environmental pollution. Therefore, the preparation of the superhydrophobic surface of some natural materials such as cellulose and biodegradable materials has become the main research direction in this year.[22] Athanasios et al.[23] prepared an environment-friendly and biodegradable superhydrophobic surface by taking the surface of a lotus leaf as a reference. The surface was mainly composed of microstructured cellulose and had good hydrophobicity and self-cleaning property. Bayer et al.[24] prepared the superhydrophobic cellulose surface by casting or dipping the solution of organic microparticles and inorganic nanoparticles. These hydrophobic polymers well covered the fiber surface and made the cellulose surface hydrophobic, which further promoted the multifunctional application of cellulose materials.

In this paper, we successfully prepared the superhydrophobic paper mulch film with easy degradation, low cost, and long service life by brushing ZnO/SiO_2 suspension on the surface of a paper base film in turn and drying for a certain period of time. The waterproof property and durability of the superhydrophobic paper mulch film are two of the bases for testing the practicability of the paper mulch film. We tested the performance of the prepared superhydrophobic paper mulch film and tested its corrosion durability, hydrophobicity, and mechanical stability. The hydrophobic property, impermeability, and service life of hydrophobic paper were investigated. The results showed that the superhydrophobic paper mulch film had excellent waterproof property and impermeability, excellent mechanical stability, and durability. Its performance comparison with other superhydrophobic papers is shown in Table 1. It can be seen from Table 1 that the brush method used in this experiment has a better hydrophobic, simple process, and environmental protection effect, which makes this superhydrophobic paper better applied in field coverage to promote the progress and development of agricultural production environment and production efficiency.

Table 1. Performance Comparison of Hydrophobic Paper with Different Preparation Processes

preparation method	difficulty of preparation process	hydrophobic surface contact angle	environmental protection	reference
brush method	easy	160°	good	
physical vapor deposition	easy	154°	good	Wen et al.[19]
immersion method	easy	154°	neutral	Zhang et al.[20]
in situ hydrolysis	difficult	152°	good	Wang et al.[21]

2. EXPERIMENTAL PART

2.1. Experimental Materials and Equipment. Hydrophobic nano-silica (SiO_2) with a particle size of 200 nm was purchased from Shanghai AMD Nanotechnology Co., Ltd. (China). Nanosized zinc oxide (ZnO) with a particle size of 300 nm was purchased from Shanghai AMD Nanotechnology Co., Ltd. (China). The fully degradable paper base membrane was purchased from Shandong Rebus Tobacco Co., Ltd. (China). A 50 mL measuring cylinder was purchased from Taizhou Ou Ke Mai Experimental Instrument Co., Ltd. (China). A 50 mL filter centrifuge tube was purchased from Xintai Experimental Equipment Wholesale Co., Ltd. (China). Anhydrous ethanol was purchased from Tianjin Fuyu Fine Chemical Co., Ltd. (China). A numerical control ultrasonic cleaner (KQ-500DE type) was purchased from Kunshan Ultrasonic Instrument Co., Ltd. (China). An electric blast drying oven was purchased from Shanghai Yiheng Scientific Instrument Co., Ltd. (China). Disposable droppers were purchased from Xi'an Pengzheng Biotechnology Co., Ltd. (China). A beaker was purchased from Sichuan Shubo (Group) Instrument Co., Ltd. (China). A CA tester (HKCA-15) was purchased from Beijing Hacker Test Instrument Factory (China). An interferometric three-dimensional surface topography instrument, SEM450 field emission scanning electron microscope, was purchased from NOVA-NANO Co., Ltd. (USA). A 300 mL Jinteng glass sand core filter device and a circulating water multipurpose vacuum

https://doi.org/10.1021/acsomega.1c02618
ACS Omega 2021, 6, 24407−24418

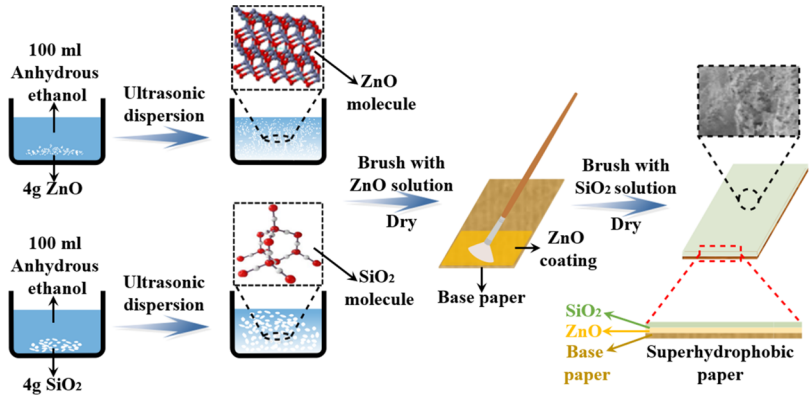

Figure 1. Preparation process of the superhydrophobic paper mulch film.

pump were purchased from Tianjin Kono Instrument Equipment Co., Ltd. (China).

2.2. Preparation of the Superhydrophobic Paper Film. The fabrication process of ZnO/SiO_2 is shown in Figure 1. First, add 100 mL of anhydrous ethanol to each of the two beakers. The 4% mass fraction nano-zinc oxide and nano-silica powders were weighed with a precision electronic scale. Then, these powders were added into absolute ethyl alcohol solution, and the beakers were placed in an ultrasonic disperser for ultrasonic dispersion for 20 min to prepare ZnO dispersion solution and SiO_2 dispersion solution.

In the first step, the nylon brush was immersed in nanosized zinc oxide dispersion solution. Then, a layer of nanosized zinc oxide dispersion solution was evenly brushed on the surface of the paper mulching film with the brush. After that, the brush was dried for 20 min in an electric air blast drying oven. The second step was to soak the nano-silica dispersion solution with a new nylon brush and then brush nano-silica dispersion solution on the paper mulching film based on nano-zinc oxide twice. The paper mulching film after brushing nano-silica dispersion solution was put into the electric heating air drying oven for 20 min, and the superhydrophobic paper mulching film was prepared after drying. The prepared superhydrophobic paper mulching film was stored in a dry place.

2.3. Performance Test and Characterization Analysis. *2.3.1. Static Infiltration.* The paper mulch film used in this experiment was divided into treated and untreated parts. The prepared superhydrophobic paper and base paper were pressed into circular sheets with a diameter of 10 mm, which were put into the bottom of the centrifuge tube with tweezers, and the sealing ring clamped them tightly. Then, 10 mL of distilled water was added into the centrifuge tube with a measuring cylinder and placed at room temperature. The water permeability of two control groups (five samples in each group, the average value of water permeability of five samples) and two control groups (five samples in each group, the average value of water permeability of five samples in each group, the average value of water permeability of five samples in each group) and the roll-off angle (RA) and water contact angle (CA) of the hydrophobic surface after static infiltration were observed respectively at 48, 96, 144, 192, and 240 h.

2.3.2. Negative Pressure Infiltration. The paper mulch film used in this experiment was divided into treated and untreated parts. The treated paper mulch film was single-sided hydrophobic paper coated with a hydrophobic coating by a glossy surface (the reverse side is not hydrophobic). The prepared superhydrophobic paper and base paper were respectively pressed into a square with a uniform specification of 3 cm × 3 cm, which were placed on the sand core filter head. The funnel filter cup and sand core filter head were clamped and fixed with stainless steel fixing clips and placed on a triangular liquid-collecting bottle. Add 50 mL of distilled water into the funnel filter cup with a measuring cylinder, turn on the vacuum pump, adjust the vacuum degree to 0.01, 0.02, and 0.03 MPa, respectively, and observe the water permeability after 20 min. In this experiment, the water permeability, hydrophobicity, self-cleaning, and surface morphology changes of the base paper were tested.

2.3.3. Wet Strength Test. A tensile tearing tester was used to tear tensile samples (dumbbell-shaped according to GB/T528-2009) and five right-angled samples (right-angled according to GB/T529-2008) after soaking for different times and air-drying at room temperature for 15 min. After tensile tearing, the average tensile tearing strength of five groups of samples was calculated, which reduced the chance of experiment and increased the persuasiveness of experiment.

2.3.4. Characterization Analysis. The SEM450 field emission scanning electron microscope of NOVANANO Company of America was used to characterize the surface and cross-section morphology of the samples after tensile tearing. The acceleration voltage was 10 kV, and the surface and cross section were observed after gold spraying treatment (which can enhance their conductivity and make the morphology clearer). The surface element distribution content of the soaked samples was comprehensively analyzed, and then the tensile tearing strength was better explained and analyzed from the microscopic aspect.

3. RESULTS AND DISCUSSION

3.1. Characterization Analysis. Figure 2 shows the scanning electron microscopic images of the surface morphology of superhydrophobic paper, and Figure 2a,b shows that SiO_2 presents an irregular phosphorus flake, and SiO_2 is a three-dimensional network structure formed with a silicon-

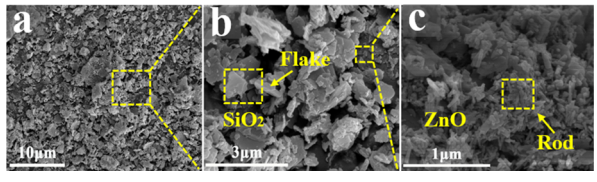

Figure 2. (a−c) Surface scanning electron microscopic images.

https://doi.org/10.1021/acsomega.1c02618
ACS Omega 2021, 6, 24407−24418

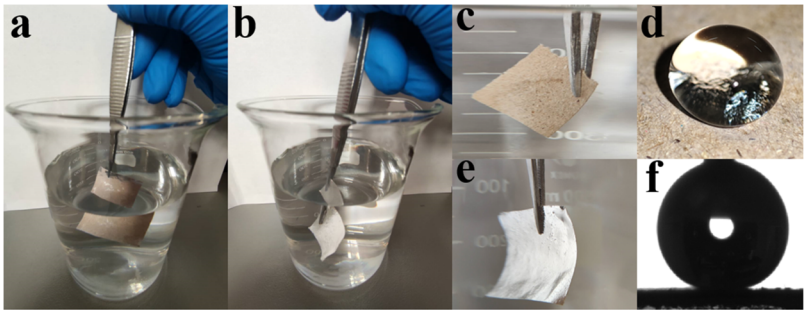

Figure 3. (a, b) Paper immersion diagram. (c) Base paper immersion in water does not lead to a mirror-like phenomenon. (d) Water drops that fall on the surface of hydrophobic paper after immersion are spherical. (e) Hydrophobic paper immersion in water leads to a mirror-like phenomenon. (f) Optical photo of water droplets falling on the surface of hydrophobic paper.

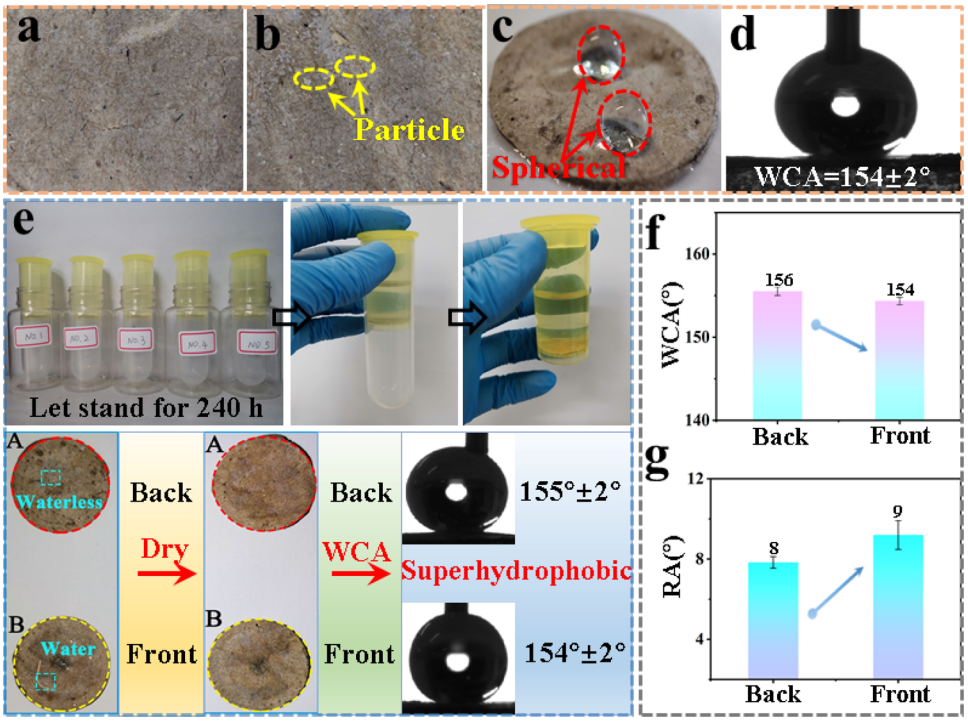

Figure 4. (a) Hydrophobic paper without standing infiltration and (b) after 240 h infiltration. (c) Drops of water on the surface of hydrophobic paper are spherical. (d) After standing infiltration, the hydrophobic paper CA is 154 ± 2°. (e) State diagram of hydrophobic paper after standing infiltration for 240 h. (f) CA after standing infiltration for 240 h. (g) RA after standing infiltration for 240 h.

oxygen tetrahedron as the basic structure. In the crystal structure, the Si atom is the center of the regular tetrahedron, the O atom is the vertex of the tetrahedron, each silicon atom is connected with four oxygen atoms, and each oxygen atom is connected with two silicon atoms. This special chemical structure endows it with excellent hydrophobic properties.[25] Figure 2c shows that ZnO presents a bar-like structure arranged one by one, which is combined with each other and presents a concave-convex shape, with a hydrophobic surface and good mechanical stability, which is beneficial to improve the mechanical stability and tensile resistance of the paper mulching film.

3.2. Influence of Different Permeations on Hydrophobicity. *3.2.1. Contact Angle (CA) and Rolling Angle (RA) Tests.* The mirror surface phenomenon generally refers to the coating surface treated with particles like SiO_2 as additives that is soaked in distilled water for a period of time, and then, due to the establishment of the solid−liquid−gas three-phase interface on the coating surface, particles gradually appear on the surface and present a mirror-like phenomenon.[26] The effects of the soaking original paper mulch film and hydrophobic paper mulch film in water are shown in Figure 3a,b, respectively; when hydrophobic paper is immersed in a certain amount of distilled water with tweezers, an air layer will be formed between water and the paper surface due to the existence of a coating, compared with the original paper mulch film in Figure 3c, a mirror phenomenon can be observed, as shown in Figure 3e, and an obvious mirror surface phenomenon can be observed. In contrast to this phenomenon, after the base paper is immersed in water, there is no mirror surface phenomenon, and even its surface is partially wetted. Through the comparison of two kinds of paper phenomena, it can be seen that hydrophobic paper has good hydrophobic performance. It can be seen from the macroscopic picture of Figure 3d that the water drops are placed on the soaked hydrophobic paper in a spherical shape. According to the optical photo of contact Angle in Figure 3f, it can be seen that the contact Angle of the soaked hydrophobic paper

https://doi.org/10.1021/acsomega.1c02618
ACS Omega 2021, 6, 24407−24418

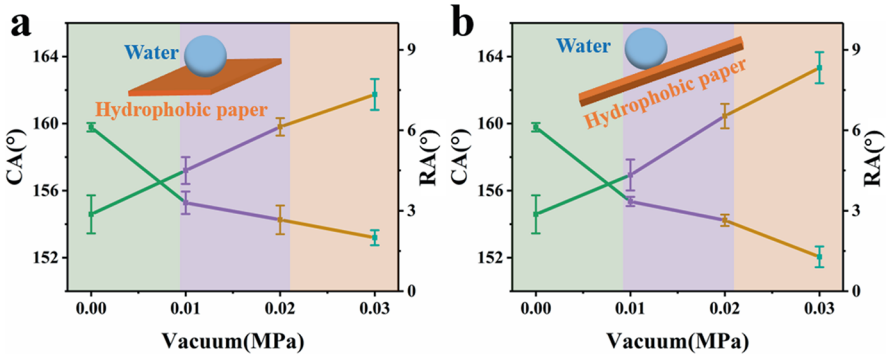

Figure 5. (a) Change in CA and RA on the front side after negative pressure and (b) change in CA and RA on the back side after negative pressure.

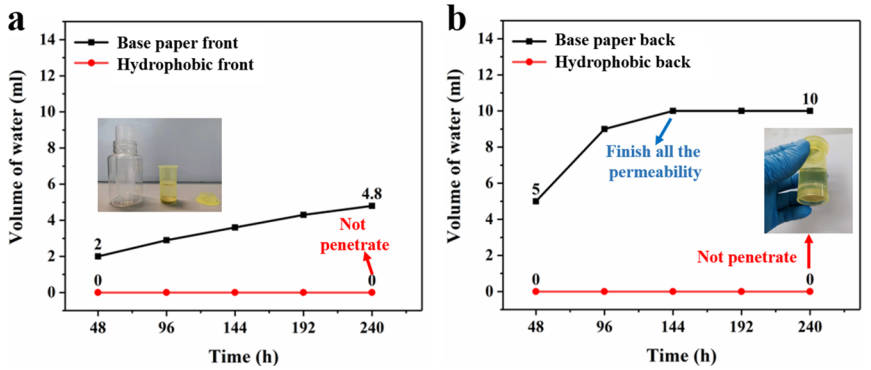

Figure 6. (a) Changes in water permeability at different times when the base paper faces up and the hydrophobic paper faces up (hydrophobic paper faces up) and (b) changes in water permeability at different times when the base paper faces up and the hydrophobic paper faces up (nonhydrophobic paper faces up).

surface is greater than 150°, which has good hydrophobicity, and also well explains the mirror phenomenon mentioned above.

The hydrophobicity after standing infiltration is shown in Figure 4. It can be seen from Figure 4a,b that the surface coating of hydrophobic paper after standing infiltration for 240 h drops slightly compared with that of hydrophobic paper without standing infiltration, and the aggregates of silica particles gradually change from completely covering the surface of the paper mulching film to being dispersed and evenly distributed on the surface of the paper mulching film, forming numerous concave bodies. The micrometer-sized silica aggregates on the coating are almost completely soaked away, and only the nanosized silica particles and their aggregates are still fixed on the paper mulch film. Due to the loss of the combination of micro- and nanostructures, the contact angle of the coating gradually decreases, but the nanoagglomerates still fixed on the paper mulching film make the coating retain a certain roughness without losing the superhydrophobicity, and the coating still has the superhydrophobicity. It can be seen from Figure 4c that after drying the hydrophobic paper in the air-drying box at 50 °C for 15 min, the water drops are approximately spherical on the surface of the hydrophobic paper. When the hydrophobic paper is moved, the water drops roll off immediately, leaving no trace on the surface of the hydrophobic paper. Figure 4d shows that the CA of the hydrophobic paper surface measured by the CA tester is 154 ± 2°, thus verifying its excellent hydrophobicity. After water penetration for 240 h, the hydrophobic paper was taken out and dried in an air-drying box at 50 °C for 15 min, and the CA was measured. Figure 4e shows a state diagram after standing and permeating. Due to the existence of the hydrophobic coating, an air layer will be formed between the paper surface and water, which plays an insulating role and prevents water from entering. Therefore, water still does not drip after standing and permeating for 240 h. After taking out the hydrophobic paper and drying it in an air-drying box at 50 °C for 15 min, the hydrophobicity was still good by the CA tester. It can be seen from Figure 4f,g that the CA decreases by 2° compared with that of the reverse side, but it is still greater than 150°, the RA increases from about 8° to about 9°, and the performance decreases, but the angle is still less than 10°, which shows that the hydrophobic paper has good stability.

Figure 5a shows the contact angle and rolling angle change of the hydrophobic paper sample after exposure to negative pressure on the front for 20 min. It can be seen that the contact angle of hydrophobic paper under the condition of no negative pressure is 160°, and after exposure to the vacuum degree of negative pressure of 0.01 MPa, the contact angle of the hydrophobic paper surface becomes 155°, and the contact angle decreases to a certain extent. With the increase in the vacuum degree of negative pressure, the contact angle gradually decreases. It can be seen from the figure that the rolling Angle also presents a gradual increase trend with the increase of negative pressure vacuum degree. This is because after the coated paper and plastic film is under negative pressure, the coating with weak adhesion between some fiber gaps will slightly fall off, and the air layer produced by this part of the coating and water is not enough to support the pressure difference generated above, so some parts will break and cause holes. The CA decreased, and water drops on the hydrophobic paper after exposure to negative pressure will also produce a

https://doi.org/10.1021/acsomega.1c02618
ACS Omega 2021, 6, 24407−24418

certain lag, resulting in the increase in RA. However, even after exposure to a negative pressure of 0.03 MPa vacuum, the CA is still greater than 153°, and the RA is less than 10°; the hydrophobic paper sample still has excellent hydrophobic properties, meeting the requirements of superhydrophobicity. Figure 5b shows the change in CA and RA after exposure to negative pressure on the reverse side for 20 min. Under the condition of negative pressure vacuum degree of 0.01 MPa, the surface contact angle of hydrophobic paper becomes155.35°, which is smaller than that of hydrophobic paper without negative pressure. This shows that the contact angle gradually decreases with the increase of vacuum degree. In addition, it can be seen from the figure that the rolling angle of hydrophobic paper gradually increases with the increase of vacuum degree. Because the paper mulch is in direct contact with the water soak process, which can cause the paper inside the fiber to be wetted, and with the increase in pressure, the water contact area of the paper inside the fiber will further increase. As a result, the nano-particles with weak adhesion on the fiber surface will partially fall off, which will lead to the decline of hydrophobic properties of hydrophobic paper, and then the contact angle of hydrophobic paper will decrease with the increase of osmotic pressure. The rolling angle also has lag due to this reason, so the rolling angle increases. It can be seen in the figure, compared with the positive pressure. The reverse negative pressure angle decreased slightly more. After exposure to the vacuum negative pressure of 0.03 MPa, the CA was still greater than 150° and the RA was less than 10°. Through comparison and verification of the two test methods, it can be seen that the hydrophobic properties of the hydrophobic paper sample were excellent.

3.2.2. Permeability Test. It can be seen from Figure 6a that after standing at room temperature for 240 h, the water permeability of the base paper is 4.8 mL, while the hydrophobic paper will form an air layer at the water−paper interface, which plays an insulating role, and the water permeability of the hydrophobic paper on the coating surface is 0 mL, which is completely impermeable. By comparison, it can be seen that the coating improves the hydrophobicity of the paper. It can be seen from Figure 6b that after standing at room temperature for 240 h, the water permeability of base paper with the smooth side facing down is 10 mL in 144 h, while that of hydrophobic paper with the coated side facing down is 0 mL. The hydrophobic paper has excellent hydrophobic characteristics and antiseepage property, which can improve the service life of the paper mulching film in a wet environment and has a good practical value.

As shown in Figure 7, it is a comparative diagram of negative pressure water permeability changes between the front side (hydrophobic coated side facing up) and the back side (nonhydrophobic side facing up) of hydrophobic paper and base paper. It can be clearly seen from the figure that the water permeability of base paper is 0.5 mL after standing at 0 MPa for 20 min, while the water permeability of both sides of hydrophobic paper is not. With the increase in negative pressure vacuum degree, the water permeability of base paper gradually increases, reaching 50 mL at 0.02 MPa. Water in the funnel filter cup is reduced to 0, water permeates from the reverse side when the vacuum degree is 0.01 MPa, and the water permeability from the reverse side when the vacuum degree is 0.03 MPa is 13 mL. When the vacuum degree is 0.03 MPa, the water permeability from the front side is 4 mL. Compared with the former two, the water permeability from

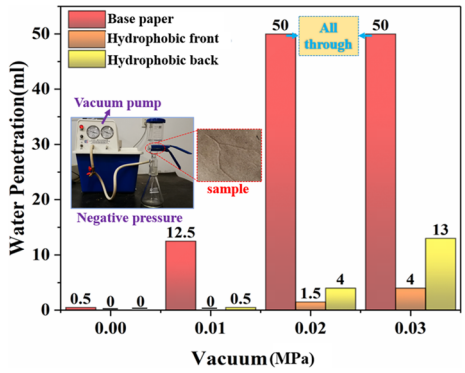

Figure 7. Comparison of negative pressure permeability of hydrophobic paper on the front side (hydrophobic surface up) and on the back side (nonhydrophobic surface up) and base paper.

the front side is less. It will have a certain supporting force with the air layer generated by water, and water is resistant and difficult to penetrate under negative pressure. Therefore, it can be seen that the coating improves the water-repellent performance of the paper mulching film, and it is more difficult to penetrate rain than the original paper. Compared with the base paper, the superhydrophobic paper mulch film has better antipermeability than the base paper, which makes the paper mulch film have a better ability to adapt to a complex agricultural environment.

3.2.3. Self-cleaning Test of Samples after Exposure to Negative Pressure. Figures 8 and 9 respectively show the clean experimental schematic diagram and the testing figure, Figure 9a shows the base paper self-cleaning, Figure 9b−d shows the self-cleaning of base paper after exposure to different vacuum negative pressures with the front side facing up, Figure 9e shows the hydrophobic paper without negative pressure from the cleaning, and Figure 9f−h shows the hydrophobic paper on the opposite face after exposure to different vacuum negative pressures after the cleaning. Soil particles were evenly scattered on the surface of the paper, and 15 μL water droplets were dropped on the soil particles with a dropper. As can be seen from Figure 9a, the liquid droplets presented a viscous state on the base paper, and the water droplets did not clean the soil stains on the surface of the paper, which indicated that the self-cleaning performance of the base paper was poor. Water droplets on the front side of the hydrophobic paper with different vacuum and negative pressure of Figure 9b−d can clean up the soil particles on the surface.This shows that the hydrophobic paper still has good self-cleaning performance after negative pressure. Drops of water on the reverse-side suction sample in Figure 9f−h also appear to clean the path, and Figure 9e shows hydrophobic paper without negative pressure since the cleaning efficiency is visible after exposure to different vacuum negative pressures and the drain cleaning efficiency on the surface of the paper is still good.

3.3. Surface Topography Analysis of Negative Pressure Infiltration. *3.3.1. Electron Microscopy Diagram after Exposure to 0.03 MPa Vacuum Degree Negative Pressure.* Figure 10 shows an electron micrograph of the surface after exposure to negative pressure on the hydrophobic coating surface and negative pressure on the nonhydrophobic surface. From the electron micrograph, it can be seen that after exposure to a negative pressure of 0.03 MPa on the hydrophobic coating surface for 20 min, as shown in Figure 10a−c, there are fewer holes on the hydrophobic paper surface.

https://doi.org/10.1021/acsomega.1c02618
ACS Omega 2021, 6, 24407−24418

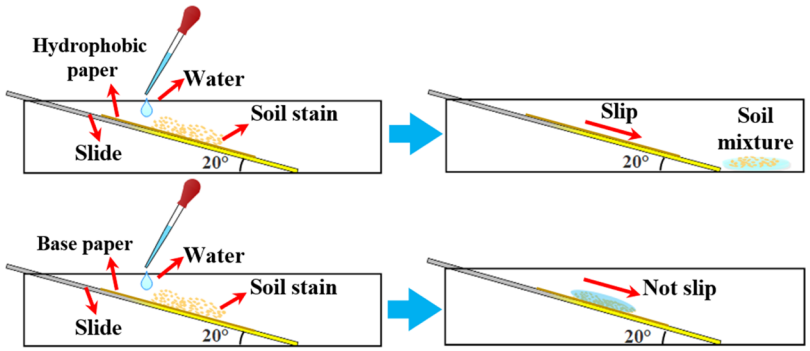

Figure 8. Self-cleaning model diagram.

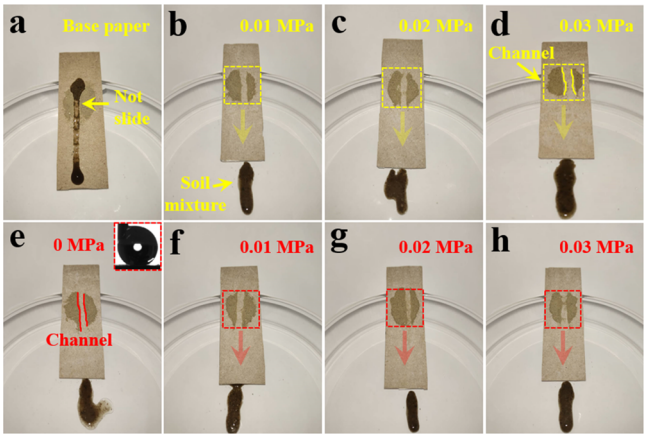

Figure 9. (a) Base paper self-cleaning, (b–d) base paper facing up after exposure to different vacuum negative pressures, (e) hydrophobic paper without negative pressure, and (f–h) hydrophobic paper facing up after exposure to different vacuum negative pressures after self-cleaning.

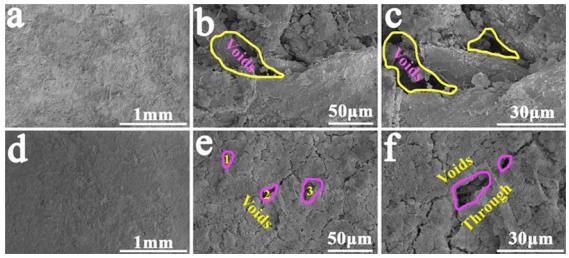

Figure 10. Electron microscopic images after exposure to 0.03 MPa vacuum negative pressure: (a–c) hydrophobic surface negative pressure upward and (d–f) nonhydrophobic surface negative pressure upward.

Under negative pressure, the pressure in the lower triangular conical liquid-collecting bottle is lower than the atmospheric pressure, resulting in a pressure difference. Because the supporting force generated by part of the air layer formed by the hydrophobic paper surface and water is not enough to resist the pressure difference, some holes are generated and there are water droplets. On the other hand, after exposure to the negative pressure of 0.03 MPa on the nonhydrophobic surface for 20 min, as shown in Figure 10d–f, there are some holes, which are slightly more than the hydrophobic surface. This is because the nonhydrophobic surface is upward, there is no air layer between water and paper, and water is in direct contact with paper fibers, which are gradually wetted. Because water is hydrophobic below, it can block water, but the paper fibers are partially wetted, and the hydrophobic powder with weak adhesion between fibers will fall off, resulting in the formation of holes.

Figure 11a shows an electron micrograph of the sample surface after exposure to a positive/negative pressure of 0.03 MPa for 20 min. The distribution of C, N, O, Zn, and Si can be clearly seen from the diagram in Figure 11b–f. It can be seen that after exposure to positive/negative pressure, the contents of Si and Zn on the surface distribution are 34 and 20%, respectively. The air layer formed by water and the hydrophobic surface can resist part of the pressure difference, and some large particles with weak surface adhesion fall off. Figure 11g shows the electron microscopic image of the surface of the sample after exposure to negative pressure for 20 min under the vacuum degree of 0.03 MPa, and Figure 11h–l shows the distribution of C, N, O, Zn, and Si. The contents of Si and Zn in the surface distribution are 29 and 15%, respectively, which are lower than those under positive/negative pressure. Because the reverse side is facing up (the nonhydrophobic side is facing up), water is in contact with paper fiber, and there is no air layer. The powder shedding is accelerated, so the content of elements is slightly lower than that under positive/negative pressure, which is also coordinated with the previous electron microscopy. It can be seen from the previous CA that the hydrophobic paper mulch film has good hydrophobic stability.

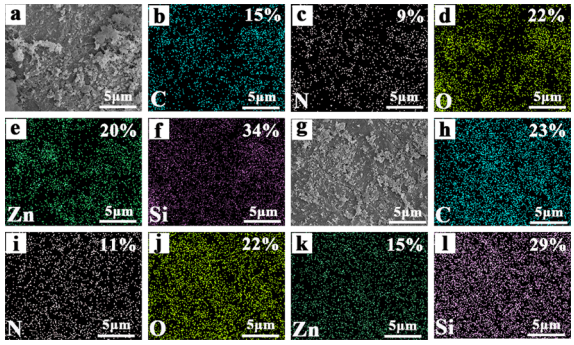

Figure 11. Negative pressure EDS diagram with a vacuum degree of 0.03 MPa. (a–f) Positive/negative pressure electron microscopic diagram with a vacuum degree of 0.03 MPa and EDS diagram with different elements; (g–l) negative pressure electron microscopic diagram with a vacuum degree of 0.03 MPa and diagram with different element contents.

https://doi.org/10.1021/acsomega.1c02618
ACS Omega 2021, 6, 24407−24418

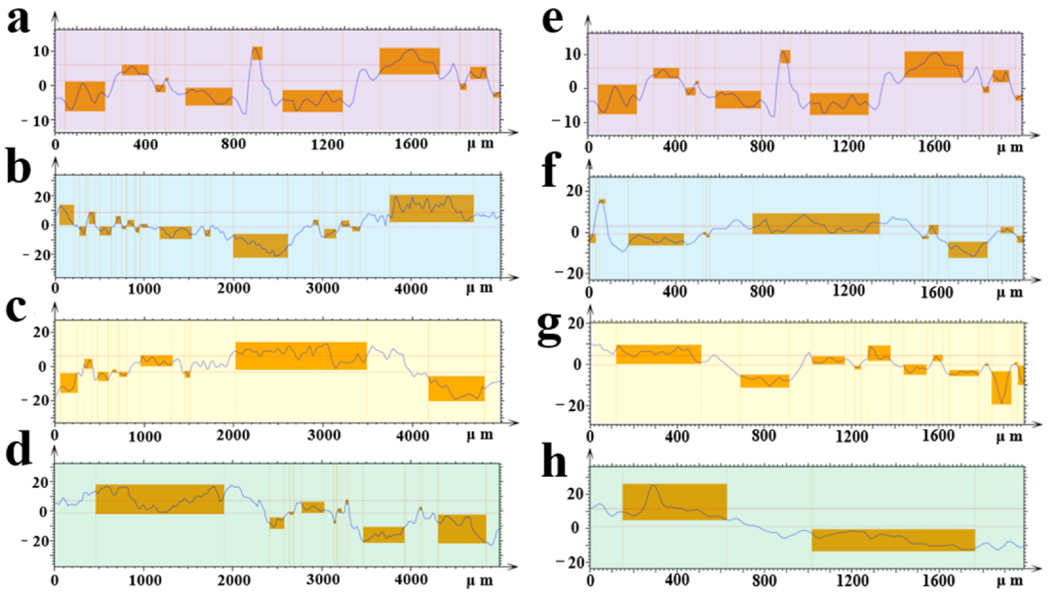

Figure 12. Negative pressure surface peaks and valleys with different vacuum degrees on the front and back: (a) front non-negative pressure hydrophobic paper, (b–d) positive/negative pressure peak-valley diagram, (e) non-negative pressure hydrophobic paper on the reverse side, and (f–h) negative pressure peak-valley diagram.

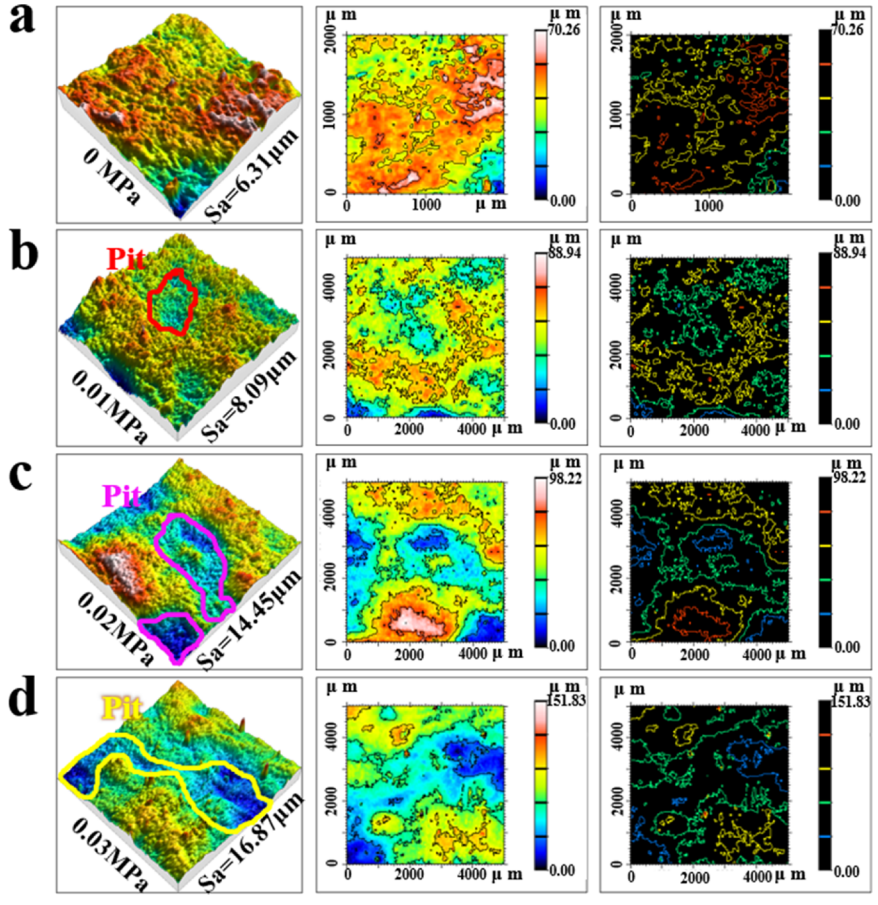

Figure 13. Three-dimensional morphology and roughness of negative pressure with different vacuum degrees on the front: (a) no negative pressure, (b) 0.01 MPa negative pressure, (c) 0.02 MPa negative pressure, and (d) 0.03 MPa negative pressure.

3.3.2. Three-Dimensional Morphology of Different Vacuum Degrees and Negative Pressures. Figure 12 shows the peak-valley map (height distribution map) of surface topography after exposure to negative pressure under different vacuum degrees on the front and back. It can be seen from Figure 12a–d that after exposure to negative pressure on the front, more pits are produced on the surface, which increases the height difference and roughness. This is because when

https://doi.org/10.1021/acsomega.1c02618
ACS Omega 2021, 6, 24407–24418

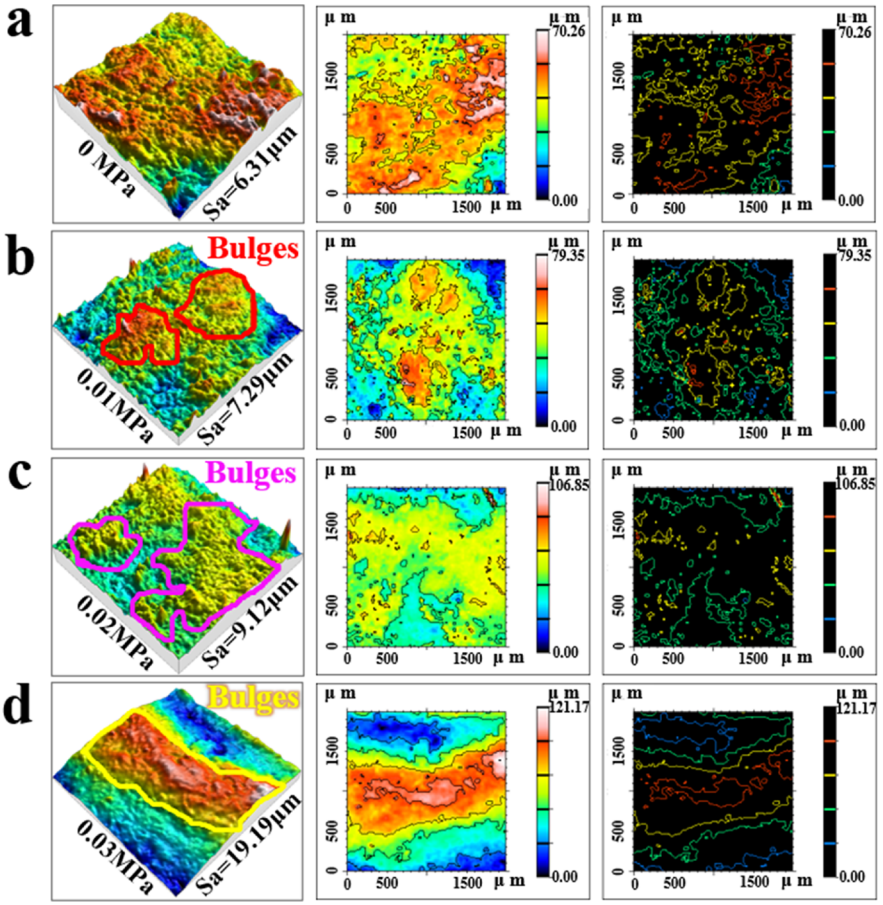

Figure 14. Three-dimensional morphology and roughness of negative pressure with different vacuum degrees on the reverse side: (a) no negative pressure, (b) 0.01 MPa negative pressure, (c) 0.02 MPa negative pressure, and (d) 0.03 MPa negative pressure.

negative pressure occurs, the pressure in the triangular conical liquid-collecting bottle is lower than the atmospheric pressure, resulting in a pressure difference. The air layer produced by water and the hydrophobic surface can only offset a small part of downward force, so the downward force causes the paper surface to bulge downward, which is concave on the hydrophobic surface. On the contrary, for the negative pressure in Figure 12e−h, because the hydrophobic surface is below, when negative pressure occurs, the upper nonhydrophobic surface is concave, while the hydrophobic surface is convex. After exposure to negative pressure, the hydrophobic performance is still good, the surface is basically complete, and the hydrophobic paper has good mechanical stability. It can also be seen that the hydrophobic paper has an excellent ability to cope with a complex agricultural environment.

Figure 13a−d shows the change in surface roughness of samples after exposure to negative pressure for 20 min under different vacuum degrees. It can be seen that the surface roughness of hydrophobic paper is 6.31 μm without negative pressure. When the vacuum pump is vacuumized, the roughness is 8.09 μm and slightly increases when the vacuum degree in the triangular conical liquid-collecting bottle is 0.01 MPa. With the gradual increase in negative pressure vacuum degree, it can be seen that some pits are formed on the surface of the sample, and the roughness increases. When the vacuum degree is 0.03 MPa, the roughness is 16.87 μm. The roughness is increasing, because the supporting force provided by some air layers on the surface of hydrophobic paper is not enough to resist the pressure difference, some holes are formed, and some pits are formed on the surface of hydrophobic paper, which causes the vertical distance between the highest point and the lowest point of the surface to increase. Therefore, the roughness increases with the increase in negative pressure vacuum degree.

Figure 14a−d shows the change in three-dimensional morphology and roughness of the sample surface after exposure to negative pressure for 20 min under different vacuum degrees on the reverse side (nonhydrophobic side facing up). It can be seen that the surface roughness of hydrophobic paper is 6.31 μm without negative pressure. When the vacuum pump is vacuumized, the roughness is 7.29 μm when the vacuum degree in the triangular conical liquid-collecting bottle is 0.01 MPa. With the gradual increase in negative pressure vacuum degree, some convex needle-like shapes are formed on the surface, and the roughness of the sample increases to a greater extent than that of the front facing upward (hydrophobic side faces upward). When the vacuum degree is 0.03 MPa, the roughness is 19.19 μm, the reverse side of the sample faces upwards (nonhydrophobic side faces upwards), and water and paper fibers are in contact with each other. The wetted paper fibers will accelerate the peeling off of unstable powder on the surface, leading to the formation of holes, and the number of holes is greater than that facing upward. Therefore, it can be observed that the negative pressure roughness on the reverse side is larger than that on the front side under the same vacuum degree, which shows

https://doi.org/10.1021/acsomega.1c02618
ACS Omega 2021, 6, 24407−24418

that the hydrophobic surface has better pressure resistance, firm and strong coating, and good comprehensive performance.

3.4. Wet Strength Test. *3.4.1. Electron Micrograph of Tensile Fracture after Immersion.* Figure 15 shows an

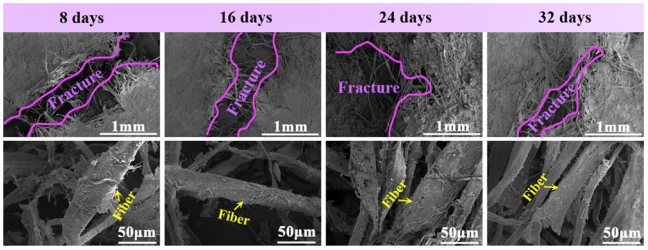

Figure 15. Fracture electron micrographs of hydrophobic paper soaked in different times.

electron micrograph of the fracture of hydrophobic paper with 4% silica content after soaking for different times and airing. Through the electron microscope, it can be seen that there is still more powder on the hydrophobic paper fiber after soaking for 8 days, and the particulate matter can be clearly seen. With the extension of soaking time, the hydrophobic powder becomes sparse in turn. By 32 days, the surface of the paper fiber is smaller and smoother than that after soaking for 8 days. The matrix of the paper fiber can be seen slightly. As the coating becomes thinner, the gaps between the fibers become wider and the maximum tensile tearing force that can be sustained by the same material increases. This is due to the decrease in fiber diameter and coating. However, despite the decrease in large particles of hydrophobic substances on the fiber surface, there are still many nanohydrophobic powders on the surface, which still possess hydrophobicity to isolate water molecules, and the CA is greater than 150°. This shows that hydrophobic paper has good stability and good wet strength. Figure 16 shows the EDS diagram of the sample at 200 μm,

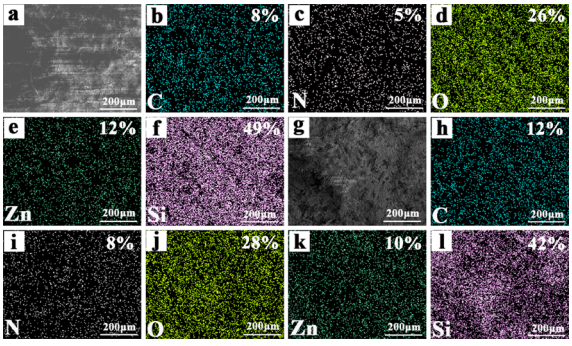

Figure 16. EDS diagram of the sample surface: (a−f) EDS diagram of the sample surface soaked for 8 days; (g−l) EDS diagram of the sample surface soaked for 32 days.

Figure 16a−f shows the element distribution diagram after soaking for 8 days, and Figure 16g−l shows the element distribution diagram after soaking for 32 days with hydrophobic paper. It can be seen that the contents of Zn and Si decreased after 32 days compared with those after 8 days, but most of the powders still adhered firmly, which had little effect on hydrophobicity.

3.4.2. Tensile Properties under Different Soaking Times. Figure 17a shows the tensile curves of samples obtained after soaking the base paper for 0, 8, 16, 24, and 32 days, standing for 15 min, and stretching by a tensile tearing machine; it can be seen from the figure that the maximum tensile strength of the base paper before soaking is 18 N, then after soaking for 8 days, the maximum tensile strength decreases to 6.05 N, which is obvious, and the maximum tensile strength decreases in turn with the increase in soaking time. After the base paper is soaked, the paper fiber undergoes a rapid water absorption stage, which absorbs the external free water in addition to the existing water. With the extension of soaking time, fiber absorbs more and more water. After being taken out at different times and left in air for a certain period of time, due to environmental reasons, water in the paper fiber will be reduced due to evaporation and will slowly reach a water loss state from the saturation state, showing a shrinking state, and the fiber diameter will also be reduced. Therefore, as the diameter of the same area decreases during stretching, the maximum tensile force is also decreased, which explains the reason for the decrease in tensile force.

Figure 17b shows the tensile curves of samples obtained by soaking hydrophobic paper for 0, 8, 16, 24, and 32 days, standing for 15 min, and then stretching by a tensile tearing machine. The maximum tensile force of the nonsoaked hydrophobic paper is 20.63 N, which is 15% higher than that of the base paper. Due to the existence of the coating, it is hydrophobic, and the fibers themselves are not in contact with water. The existence of the coating fills some gaps between fibers, which increases the tensile strength of paper. On the other hand, the existence of the coating also increases the diameter of fibers, which are covered by the coating, and the maximum tensile force borne by the same number of fibers increases. With the extension of soaking time, the number of nanoparticles with weak adhesion on the fiber surface will decrease, and the distribution of the coating will show sparse and uniform distribution. With the extension of soaking time, the tensile strength decreases, but compared with the base paper, the tensile strength decreases much less at the same soaking time, and the maximum tensile strength is much larger than that of the base paper at the same soaking time. It can be seen that the coating improves the tensile strength of paper and the mechanical stability of paper.

Figure 18a shows the tear curves of the samples obtained after soaking the base paper for 0, 8, 16, 24, and 32 days, standing for 15 min, and tearing by a tensile tearing machine. It can be seen from the figure that the tear strength of the base paper is larger when it is not soaked. With the extension of soaking time, the maximum tear strength decreases gradually, and the displacement also decreases to a certain extent. This result also matches the tensile result of the base paper. The reason for the decrease in the maximum tear strength is also related to the water absorption and water loss of the fiber. Figure 18b shows the tear graph of the sample obtained by soaking the hydrophobic paper for 0, 8, 16, 24, and 32 days, standing for 15 min, and then tearing by a tensile tearing machine. It can be seen from the figure that the maximum tear strength of hydrophobic paper is greater than that of base paper. It can be seen that the coating improves the tear strength performance of paper. With the extension of soaking time, the tear strength decreases to some extent, but it can be clearly seen that the maximum tear strength of hydrophobic paper is greater than that of base paper under the condition of soaking for the same time. It can be seen that the coating improves the mechanical properties of the paper mulch film

https://doi.org/10.1021/acsomega.1c02618
ACS Omega 2021, 6, 24407−24418

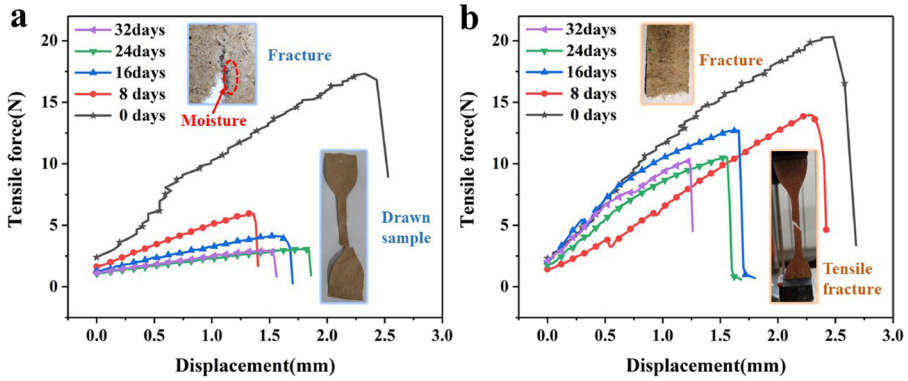

Figure 17. Plot of tensile curve of soaking at different times. (a) Tensile curve of soaking at different times for base paper; (b) tensile curve of soaking at different times for hydrophobic paper.

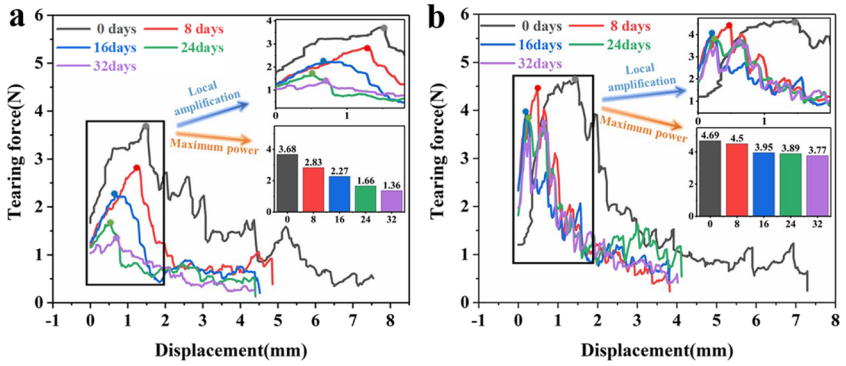

Figure 18. Tear curves of different soaking times: (a) tear and amplification curves of base paper at different soaking times; (b) tear and amplification curves of hydrophobic paper at different soaking times.

and also improves the adaptability and adaptability of the mulching film to a complex environment, which plays a positive role in the application of the paper mulch film.

4. CONCLUSIONS

(1) The SiO_2/ZnO superhydrophobic paper-based film prepared by a brush coating method with SiO_2 and ZnO as raw materials has a good low adhesion effect and excellent hydrophobic property, with a CA up to 160° and an RA less than 10°, showing good superhydrophobicity.

(2) The durability of hydrophobic paper was verified by the method of standing at room temperature and permeating under negative pressure. After standing at room temperature for 240 h and drying, its CA was greater than 154°, its RA was less than 10°, and its performance was excellent. Compared with base paper, hydrophobic paper has better permeability resistance. Silica particles on the surface of hydrophobic paper are stacked on each other to form a loose and rough micro/nanostructure, while air exists in pores, which will form an air layer between the paper surface and water, which plays a role in isolation and prevents water from infiltrating. When the vacuum is 0.03 MPa and the negative pressure is negative, the CA is greater than 153° and the RA is less than 10°. The hydrophobic paper in the negative pressure of water permeability is less than the base paper, which indicates that it has better hydrophobic stability.

(3) Test the mechanical properties of base paper and hydrophobic paper after soaking for different times, and get the conclusion that the mechanical properties of base paper decrease more than those of hydrophobic paper. The hydrophobic coating can improve the mechanical properties of the paper mulching film and effectively cover paper fibers to play a protective role, which makes the paper mulch film more mechanically stable and more adaptable to a complex environment. In practical production, hydrophobic paper has a great practical value.

AUTHOR INFORMATION

Corresponding Authors

Fengwei Zhang − *College of Mechanical and Electrical Engineering, Gansu Agricultural University, Lan Zhou 730070, China*; Email: zhangfw@gsau.edu.cn

Qiang He − *Key Laboratory of Surface Engineering, Anyang Institute of Technology, Anyang 455000, China*; orcid.org/0000-0003-4948-7887; Email: aystar@163.com

Authors

Anling Li − *Key Laboratory of Surface Engineering, Anyang Institute of Technology, Anyang 455000, China; College of Mechanical and Electrical Engineering, Gansu Agricultural University, Lan Zhou 730070, China*

Yaohui Zhao − *Key Laboratory of Surface Engineering, Anyang Institute of Technology, Anyang 455000, China*

Shuaiyang Ren − *Key Laboratory of Surface Engineering, Anyang Institute of Technology, Anyang 455000, China;*

https://doi.org/10.1021/acsomega.1c02618
ACS Omega 2021, 6, 24407−24418

College of Mechanical and Electrical Engineering, Gansu Agricultural University, Lan Zhou 730070, China

Fangyuan Zhang − *Key Laboratory of Surface Engineering, Anyang Institute of Technology, Anyang 455000, China; College of Mechanical and Electrical Engineering, Gansu Agricultural University, Lan Zhou 730070, China*

Complete contact information is available at: https://pubs.acs.org/10.1021/acsomega.1c02618

Funding

This research project was supported by the scientific and technological innovation talents of universities in Henan Province (19HASTIT023). The raw/processed data required to reproduce these findings cannot be shared at this time due to legal or ethical reasons.

Notes

The authors declare no competing financial interest.

REFERENCES

(1) Rocha, D. B.; de Carvalho, J. S.; de Oliviera, S. A.; dos Santos Rosa, D. A new approach for flexible PBAT/PLA/$CaCO_3$ films into agriculture. *J. Appl. Polym. Sci.* **2018**, *135*, 46660.

(2) Zhang, Y.; Han, J. H.; Kim, G. N. Biodegradable Mulch Film Made of Starch-Coated Paper and Its Effectiveness on Temperature and Moisture Content of Soil. *Commun. Soil Sci. Plant Anal.* **2008**, *39*, 1026−1040.

(3) La Fuente, C. I. A.; de Souza, A. T.; Tadini, C. C.; Augusto, P. E. D. Ozonation of cassava starch to produce biodegradable films. *Int. J. Biol. Macromol.* **2019**, *141*, 713−720.

(4) Tuteja, A.; Choi, W.; Ma, M.; Mabry, J. M.; Mazzella, S. A.; Rutledge, G. C.; McKinley, G. H.; Cohen, R. E. Designing Superoleophobic Surfaces. *Science* **2007**, *318*, 1618−1622.

(5) Kota, A. K.; Kwon, G.; Tuteja, A. The design and applications of superomniphobic surfaces. *NPG Asia Mater.* **2014**, *6*, e109.

(6) Zhou, H.; Wang, H.; Niu, H.; Gestos, A.; Wang, X.; Lin, T. Fluoroalkyl silane modified silicone rubber/nanoparticle composite: A super durable, robust superhydrophobic fabric coating. *Adv. Mater.* **2012**, *24*, 2409−2412.

(7) Seo, H. O.; Kim, K.-D.; Jeong, M.-G.; Kim, Y. D.; Choi, K. H.; Hong, E. M.; Lee, K. H.; Lim, D. C. Superhydrophobic carbon fiber surfaces prepared by growth of carbon nanostructures and polydimethylsiloxane coating. *Macromol. Res.* **2012**, *20*, 216−219.

(8) Rahmawan, Y.; Xu, L.; Yang, S. Self-assembly of nanostructures towards transparent, superhydrophobic surfaces. *J. Mater. Chem. A* **2013**, *1*, 2955−2969.

(9) Wang, B.; Zhang, Y.; Shi, L.; et al. Advances in the theory of superhydrophobic surfaces. *J. Mater. Chem.* **2012**, *22*, 20112−20127.

(10) Jiang, W.; He, J.; Xiao, F.; et al. Preparation and antiscaling application of superhydrophobic anodized CuO nanowire sur-faces. *Ind. Eng. Chem. Res.* **2015**, *54*, 6874−6883.

(11) Khalil-Abad, M. S.; Yazdanshenas, M. E. Superhydrophobic antibacterial cotton textiles. *J. Colloid Interface Sci.* **2010**, *351*, 293−298.

(12) Wei, S.; Lu, D.-X.; Sun, J.; He, Y.; Zhu, L.; Zhang, Y. L.; Xiao, F. S. Solvothermal synthesis of highly porous polymers and their controllable transition from macro/mesoporosity to meso/micro-porosity. *Colloids Surf., A* **2012**, *414*, 327−332.

(13) Xu, L.; Zhu, D.; Lu, X.; Lu, Q. Transparent, thermally and mechanically stable superhydrophobic coating prepared by an electrochemical template strategy. *J. Mater. Chem. A* **2015**, *3*, 3801−3807.

(14) Shi, Y. L.; Feng, X. J.; Yang, W.; et al. Preparation of super-hydropbobic titanium oxide film by sol−gel on substrate of common filter paper. *J. Sol-Gel Sci. Technol.* **2011**, *59*, 43−47.

(15) Gnedenkov, S. V.; Sinebryukhov, S. L.; Egorkin, V. S.; et al. Wettability and electrochemical properties of the highly hydrophobic coatings on PEO-pretreated aluminum alloy. *Surf. Coat. Technol.* **2016**, *307*, 1241−1248.

(16) Esmaeilirad, A.; Rukosuyev, M. V.; Jun, M. B. G.; van Veggel, F. C. J. M. A cost-effective method to create physically and thermally stable and storable super-hydrophobic aluminum alloy surfaces. *Surf. Coat. Technol.* **2016**, *285*, 227−234.

(17) Mokhtari, S.; Karimzadeh, F.; Abbasi, M. H.; Raeissi, K. Development of super-hydrophobic surface on Al 6061 by anodizing and the evaluation of its corrosion behavior. *Surf. Coat. Technol.* **2017**, *324*, 99−105.

(18) Li, C.; Mathew, B.; Sarah, S.; et al. Paper-Based Surfaces with Extreme Wettabilities for Novel, Open-Channel Microfluidic Devices. *Adv. Funct. Mater.* **2016**, *26*, 6121−6131.

(19) Wen, Q.; Guo, F.; Yang, F.; Guo, Z. Green fabrication of coloured superhydrophobic paper from native cotton cellulose. *J. Colloid Interface Sci.* **2017**, *497*, 284−289.

(20) Zhang, J.; Feng, H.; Zao, W.; et al. Flexible superhydrophobic paper with a large and stable floating capacity. *RSC Adv.* **2014**, *4*, 48443−48448.

(21) Wang, Q.; Xie, D.; Chen, J.; et al. Superhydrophobic paper fabricated via nanostructured titanium dioxide-functionalized wood cellulose fibers. *J. Mater. Sci.* **2020**, *55*, 7084−7094.

(22) Bayer, I. S. Superhydrophobic Coatings from Ecofriendly Materials and Processes: A Review. *Adv. Mater. Interfaces* **2020**, *7*, 2000095.

(23) Athanasios, M.; Chander, S. S.; Raoul, H.; et al. Engineering Fully Organic and Biodegradable Superhydrophobic Materials. *Adv. Mater. Interfaces* **2019**, *6*, 1801202.

(24) Bayer, I. S.; Fragouli, D.; Attanasio, A.; Sorce, B.; Bertoni, G.; Brescia, R.; di Corato, R.; Pellegrino, T.; Kalyva, M.; Sabella, S.; Pompa, P. P.; Cingolani, R.; Athanassiou, A. Water-repellent cellulose fiber networks with multifunctional properties. *ACS Appl. Mater. Interfaces* **2011**, *3*, 4024−4031.

(25) Ye, H.; Zhu, L.; Li, W.; et al. Constructing Fluorine-Free and Cost-Effective Superhydrophobic Surface with Normal-Alcohol-Modified Hydrophobic SiO_2 Nanoparticles. *ACS Appl. Mater. Interfaces* **2017**, *9*, 858−867.

(26) Cassie, A. B. D.; Baxter, S. Wettability of porous surfaces. *Trans. Faraday Soc.* **1944**, *40*, 546−551.